Supporting Information For:

Unveiling Heteroatom-Containing Carbon Dots from Soil Bacterial Extracellular Metabolites and Their Application in Toxic Cr^{6+} Detection

Contents

Figure S14. Fluorescence response of CDs upon addition of 100 μL 2mM Zn^{2+} solution and 100 μL 2 mM Cr^{6+} solution (λ_{ex}= 350 nm).
Figure S15. Fluorescence response of CDs upon addition of 100 μL 2mM Mg^{2+} solution and 100 μL 2 mM Cr^{6+} solution (λ_{ex}= 350 nm).
Figure S16. Fluorescence response of CDs upon addition of 100 μL 2mM Ba^{2+} solution and 100 μL 2 mM Cr^{6+} solution (λ_{ex}= 350 nm).
Figure S17. Fluorescence response of CDs upon addition of 100 μL 2mM Ag^{+} solution and 100 μL 2 mM Cr^{6+} solution (λ_{ex}= 350 nm).
Figure S18. Fluorescence response of CDs upon addition of 100 μL 2mM Ni^{2+} solution and 100 μL 2 mM Cr^{6+} solution (λ_{ex}= 350 nm).
Figure S19. Fluorescence response of CDs upon addition of 100 μL 2mM Hg^{2+} solution and 100 μL 2 mM Cr^{6+} solution (λ_{ex}= 350 nm).
Figure S20. Fluorescence response of CDs upon addition of 100 μL 2mM Cu^{2+} solution and 100 μL 2 mM Cr^{6+} solution (λ_{ex}= 350 nm).
Figure S21. Fluorescence response of CDs upon addition of 100 μL 2mM Fe^{3+} solution and 100 μL 2 mM Cr^{6+} solution (λ_{ex}= 350 nm).
Figure S22. Fluorescence response of CDs upon addition of 100 μL 2mM PO_4^{3-} solution and 100 μL 2 mM Cr^{6+} solution (λ_{ex}= 350 nm).
Figure S23. Fluorescence response of CDs upon addition of 100 μL 2mM $H_2PO_4^{-}$ solution and 100 μL 2 mM Cr^{6+} solution (λ_{ex}= 350 nm).
Figure S24. Fluorescence response of CDs upon addition of 100 μL 2mM F^{-} solution and 100 μL 2 mM Cr^{6+} solution (λ_{ex}= 350 nm).
Figure S25. Fluorescence response of CDs in PBS upon addition of 100 μL 2mM HCO_3^{-} solution and 100 μL 2 mM Cr^{6+} solution (λ_{ex}= 350 nm).
Figure S26. Fluorescence response of CDs in PBS upon addition of 100 μL 2mM SO_4^{2-} solution and 100 μL 2 mM Cr^{6+} solution (λ_{ex}= 350 nm).
Figure S27. Fluorescence response of CDs in PBS upon addition of 100 μL 2mM Br^{-} solution and 100 μL 2 mM Cr^{6+} solution (λ_{ex}= 350 nm).
Figure S28. Fluorescence response of CDs upon addition of 100 μL 2mM HPO_4^{2-} solution and 100 μL 2 mM Cr^{6+} solution (λ_{ex}= 350 nm).
Figure S29. Fluorescence response of CDs upon addition of 100 μL 2mM $C_2O_4^{2-}$ solution and 100 μL 2 mM Cr^{6+} solution (λ_{ex}= 350 nm).
Figure S30. Fluorescence response of CDs upon addition of 100 μL 2mM Cl^{-} solution and 100 μL 2 mM Cr^{6+} solution (λ_{ex}= 350 nm).

2S1. Instruments

UV–Vis absorbance spectra were recorded using U-3310 UV–Vis spectrophotometer. FTIR spectra were recorded on a Perkin Elmer Spectrum 2 FTIR spectrometer over a frequency range of 4000–400 cm^{-1}. To analyze the size and morphology of the CDs, Jeol 2100F Field Emission Transmission Electron Microscope (FETEM). A droplet of dilute CDs solution was placed on a copper grid and left to dry overnight in a desiccator. Horiba Scientific Fluoromax-4 Spectrofluorometer was utilized to record and analyze the fluorescent intensities using 0.8mg/1mL. The crystalline or amorphous nature of the materials was determined using powder X-ray diffraction (XRD). The analysis was conducted with a Rigaku SmartLab 9 kW X-ray diffractometer equipped with CuKα radiation (λ = 1.54 Å) over a 2θ range of 2–60 degrees. The elemental analysis of the material was executed by Field Emission Scanning Electron Microscope (FESEM) with Element EDS Detector, Make: Zeiss, Model: Sigma 300. Zeta potential was analysed using Aton Paar particle analyzer Litesizer 500. The Surface elemental composition was further confirmed through automated ultra-high vacuum (UHV) X-ray photoelectron spectroscopy, Model: Verse probell.

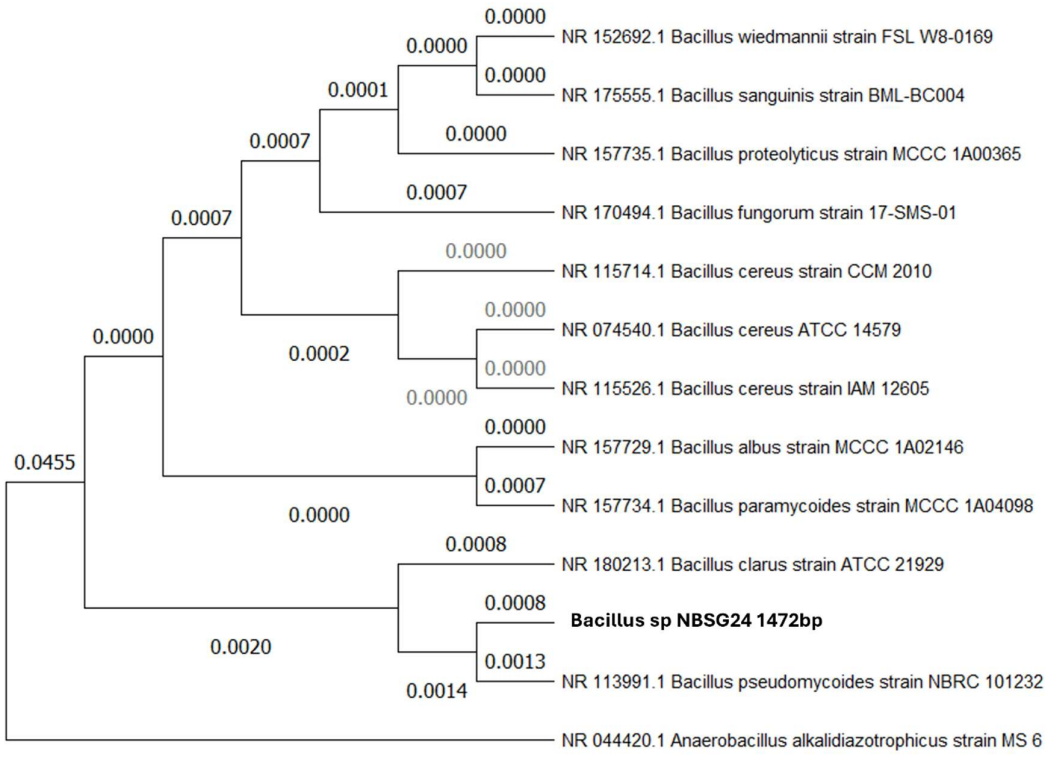

Figure S1. Phylogenetic tree of the isolated bacterium after 16S rRNA sequencing obtained through the neighbour-joining method, showing the most similarity with *Bacillus pseudomycoides* strain NBRC 101232.

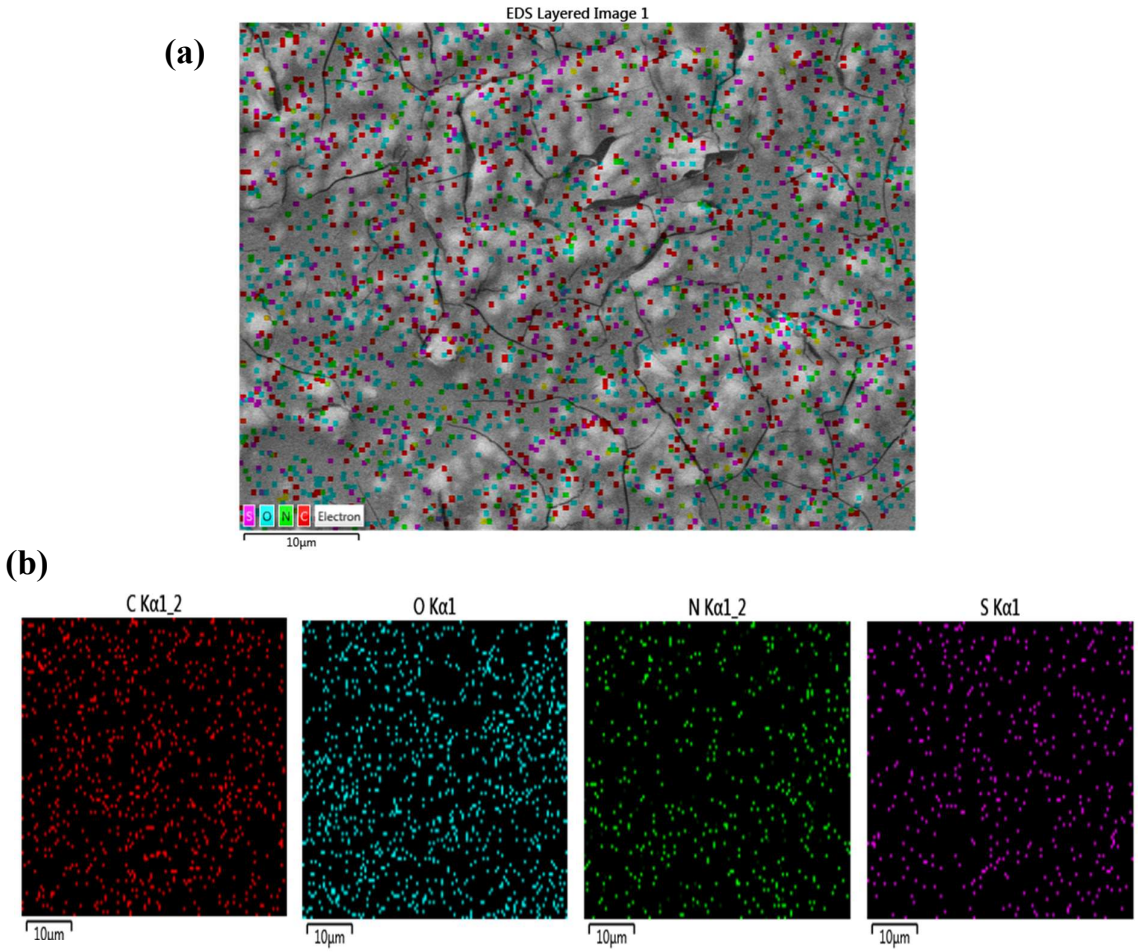

Figure S2. (a) EDS layered image, (b) EDS elemental mapping of the elements present in the CDs.

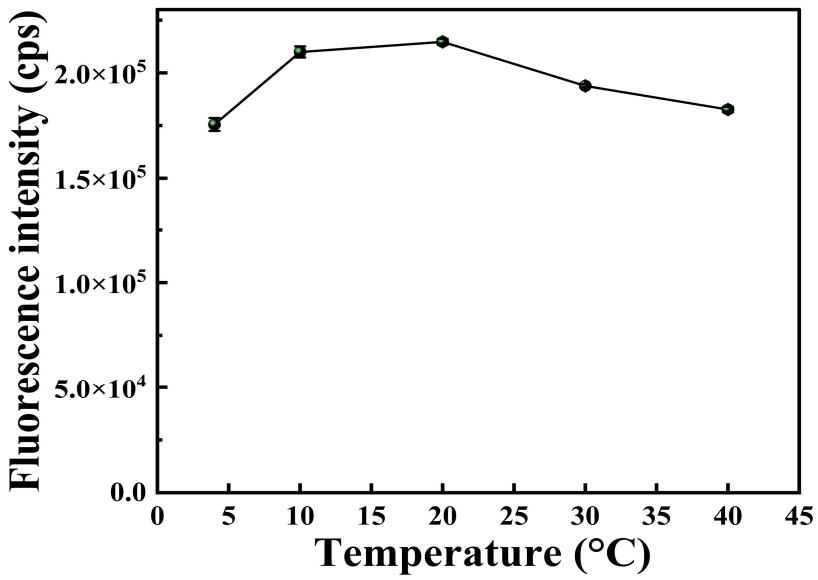

Figure S3. Fluorescence stability test of CDs under various temperatures ranging from 4°C to 40°C.

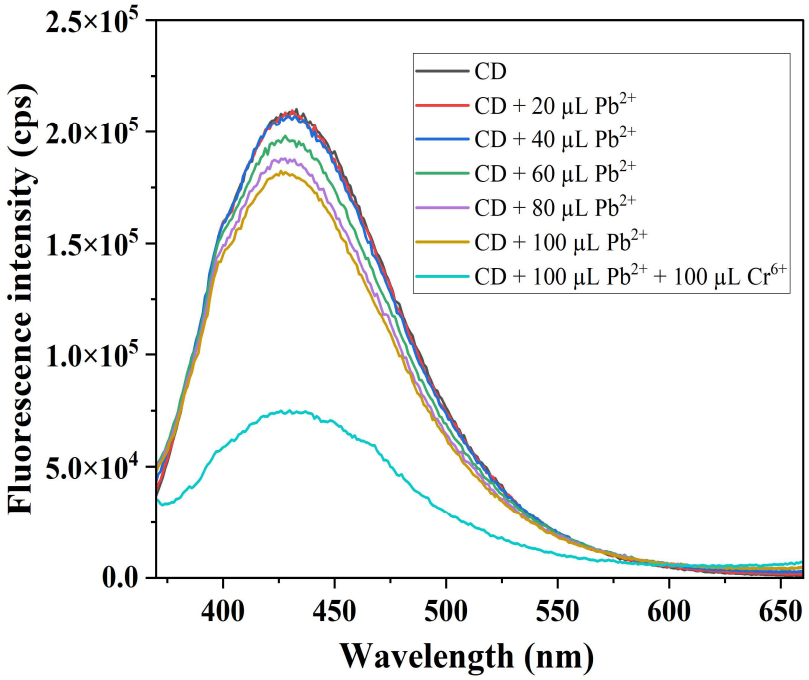

Figure S4. Fluorescence response of CDs upon addition of 100 μL 2mM Pb^{2+} solution and 100 μL 2 mM Cr^{6+} solution (λ_{ex}= 350 nm).

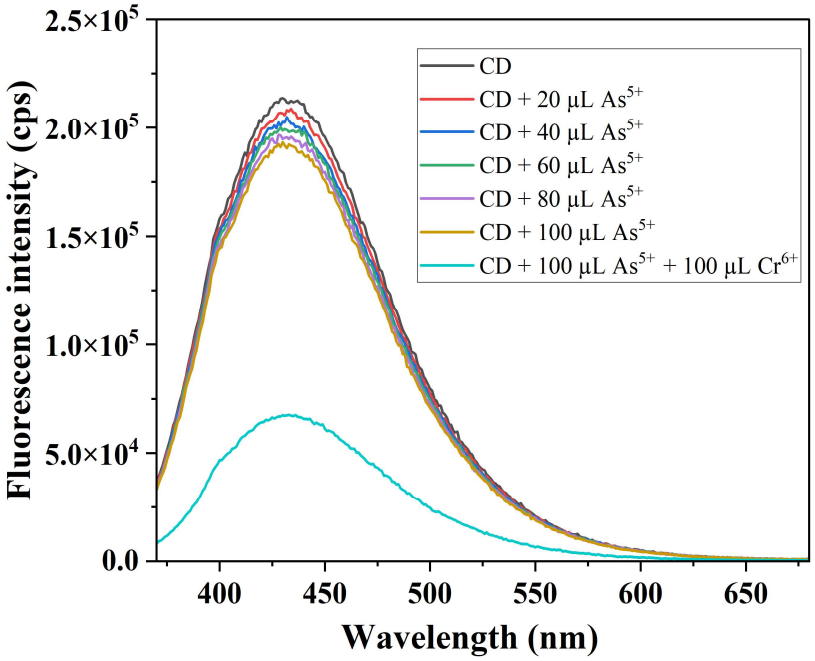

Figure S5. Fluorescence response of CDs upon addition of 100 µL 2mM As^{5+} solution and 100 µL 2 mM Cr^{6+} solution (λ_{ex}= 350 nm).

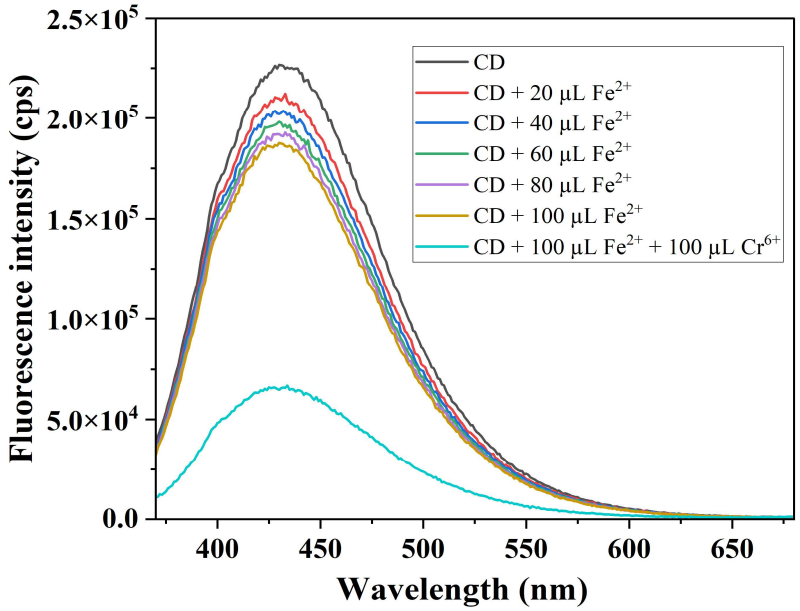

Figure S6. Fluorescence response of CDs upon addition of 100 µL 2mM Fe^{2+} solution and 100 µL 2 mM Cr^{6+} solution (λ_{ex}= 350 nm).

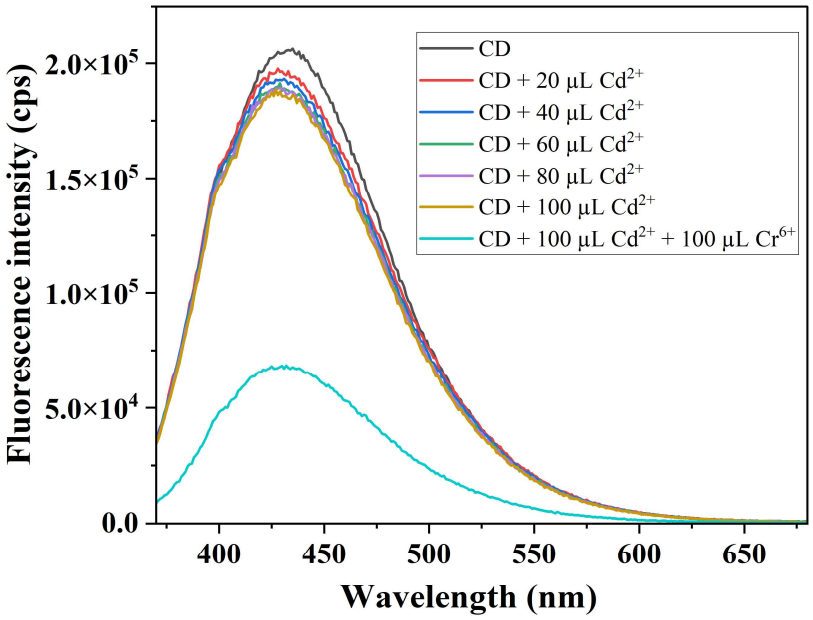

Figure S7. Fluorescence response of CDs upon addition of 100 µL 2mM Cd^{2+} solution and 100 µL 2 mM Cr^{6+} solution (λ_{ex}= 350 nm).

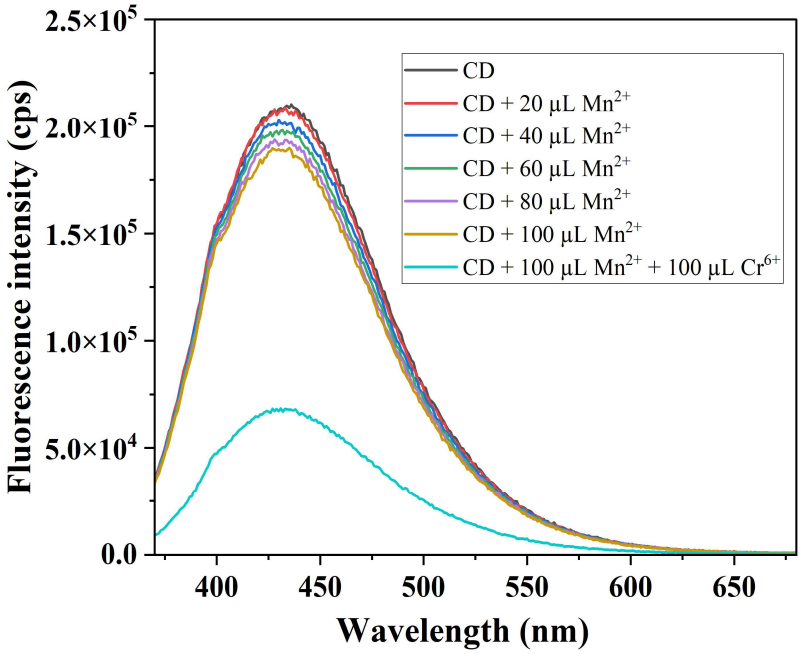

Figure S8. Fluorescence response of CDs upon addition of 100 µL 2mM Mn^{2+} solution and 100 µL 2 mM Cr^{6+} solution (λ_{ex}= 350 nm).

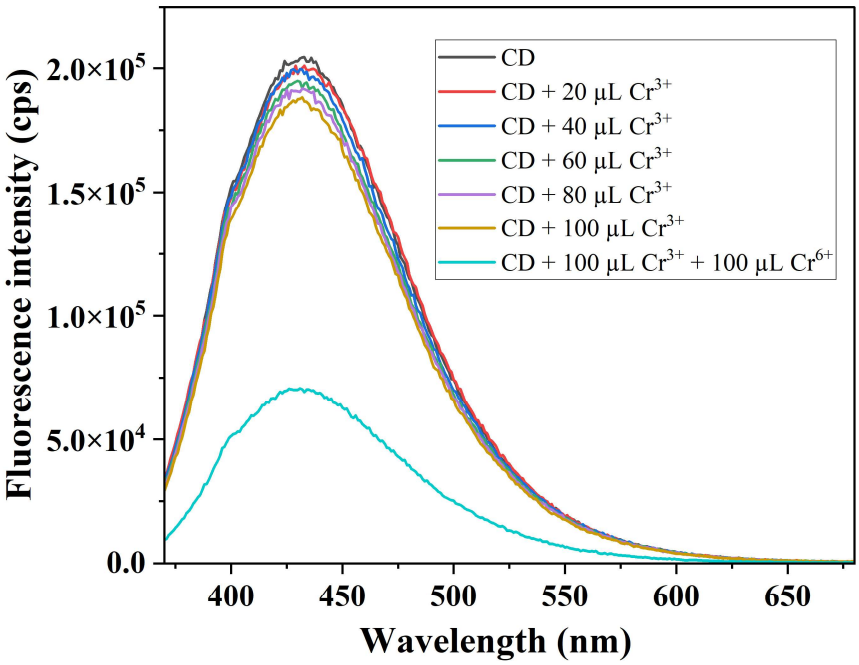

Figure S9. Fluorescence response of CDs upon addition of 100 µL 2mM Cr^{3+} solution and 100 µL 2 mM Cr^{6+} solution (λ_{ex}= 350 nm).

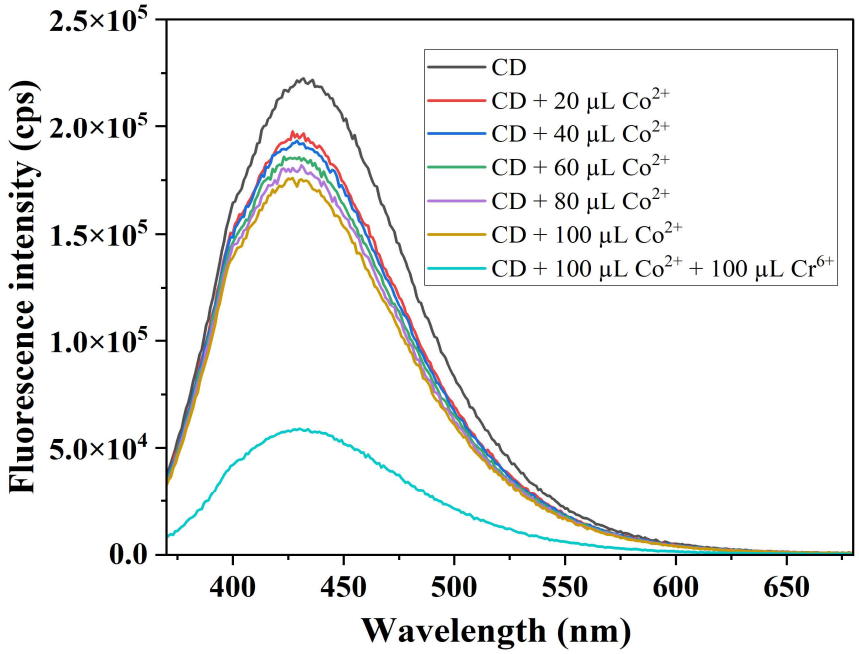

Figure S10. Fluorescence response of CDs upon addition of 100 µL 2mM Co^{2+} solution and 100 µL 2 mM Cr^{6+} solution (λ_{ex}= 350 nm).

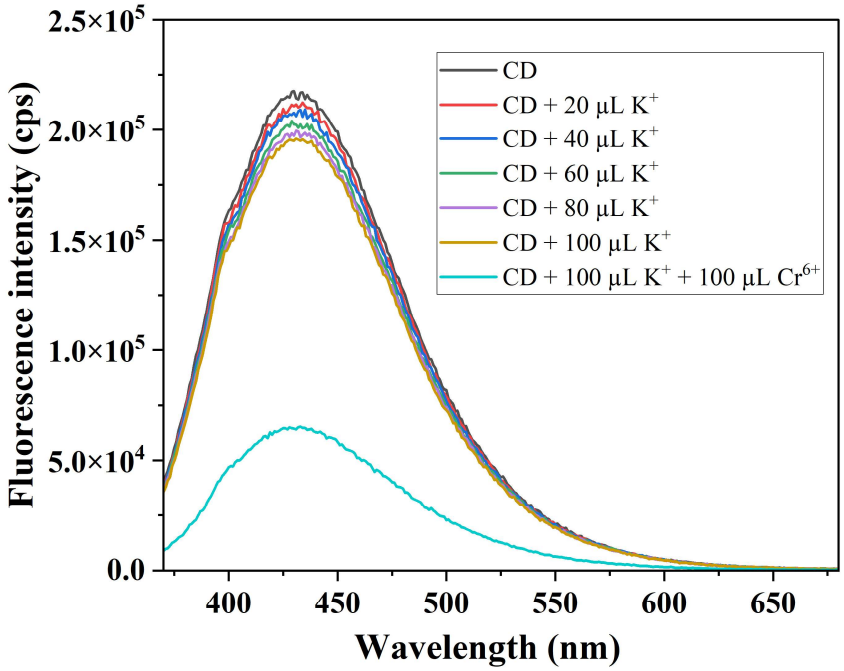

Figure S11. Fluorescence response of CDs upon addition of 100 µL 2mM K^+ solution and 100 µL 2 mM Cr^{6+} solution (λ_{ex}= 350 nm).

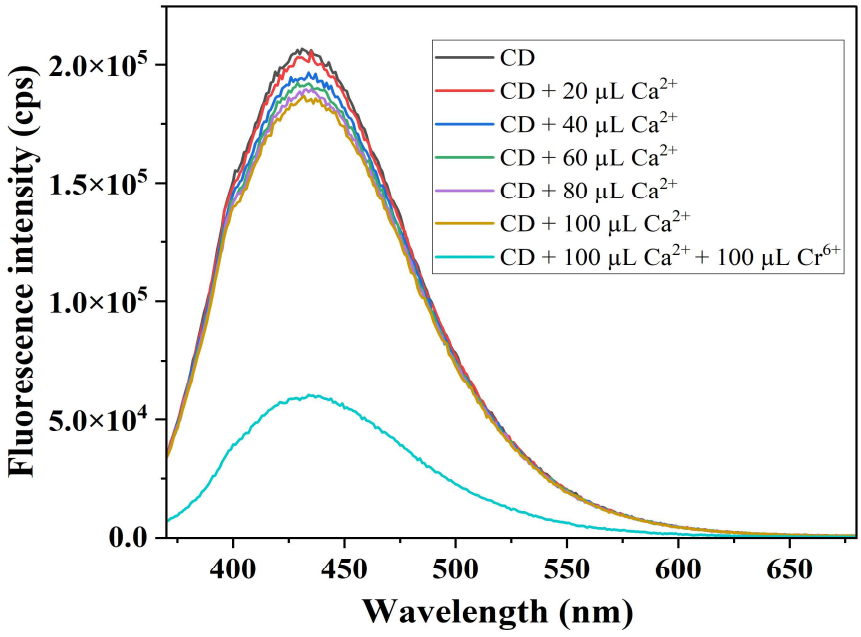

Figure S12. Fluorescence response of CDs upon addition of 100 µL 2mM Ca^{2+} solution and 100 µL 2 mM Cr^{6+} solution (λ_{ex}= 350 nm).

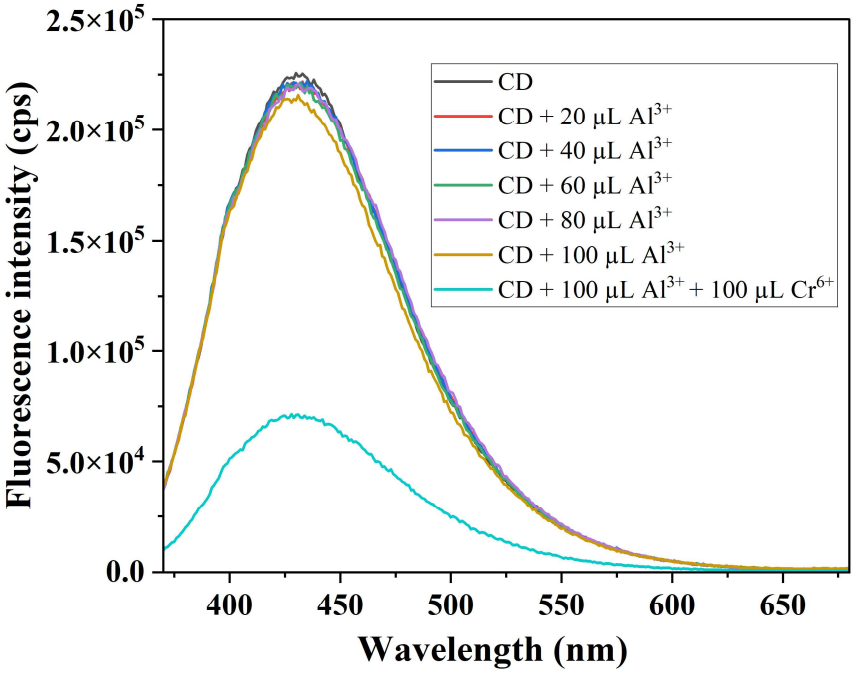

Figure S13. Fluorescence response of CDs upon addition of 100 µL 2mM Al^{3+} solution and 100 µL 2 mM Cr^{6+} solution (λ_{ex}= 350 nm).

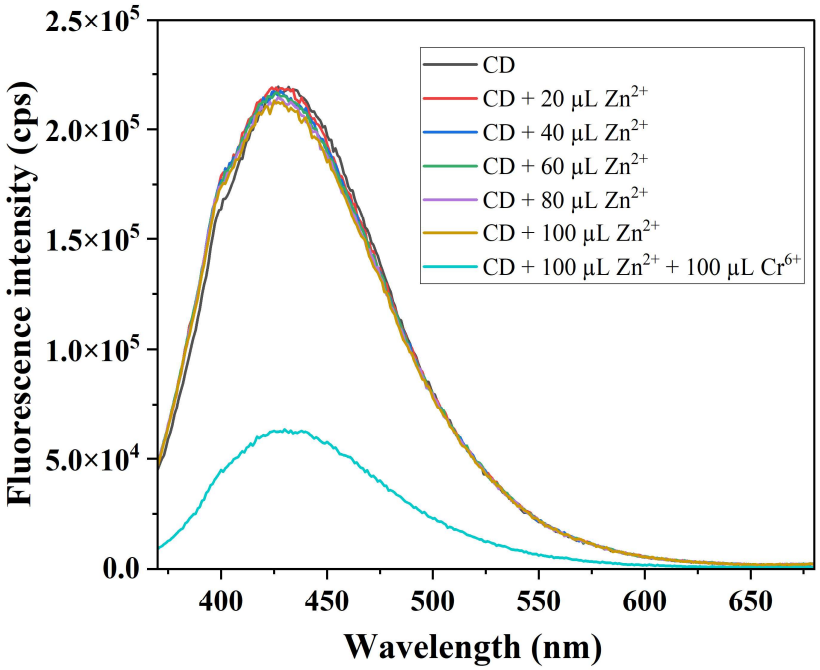

Figure S14. Fluorescence response of CDs upon addition of 100 µL 2mM Zn^{2+} solution and 100 µL 2 mM Cr^{6+} solution (λ_{ex}= 350 nm).

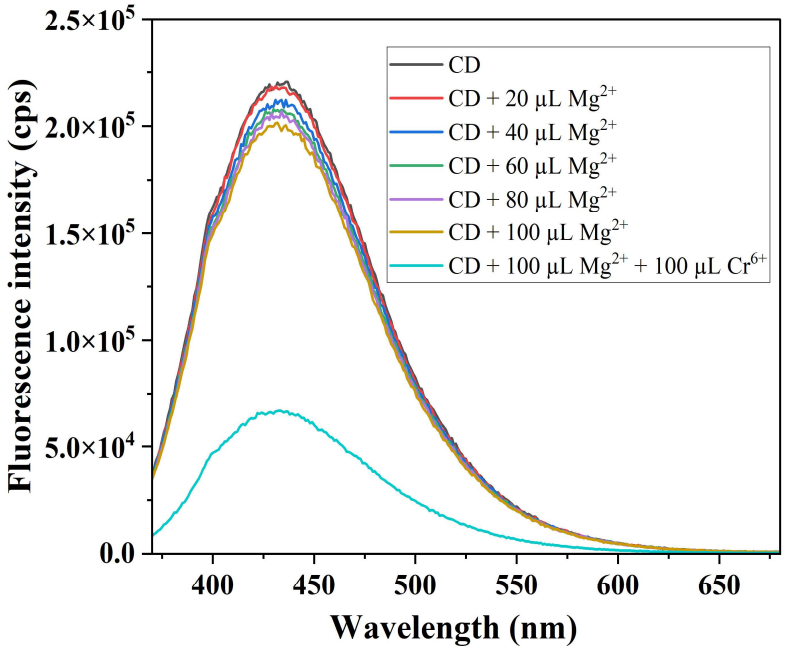

Figure S15. Fluorescence response of CDs upon addition of 100 µL 2mM Mg^{2+} solution and 100 µL 2 mM Cr^{6+} solution (λ_{ex}= 350 nm).

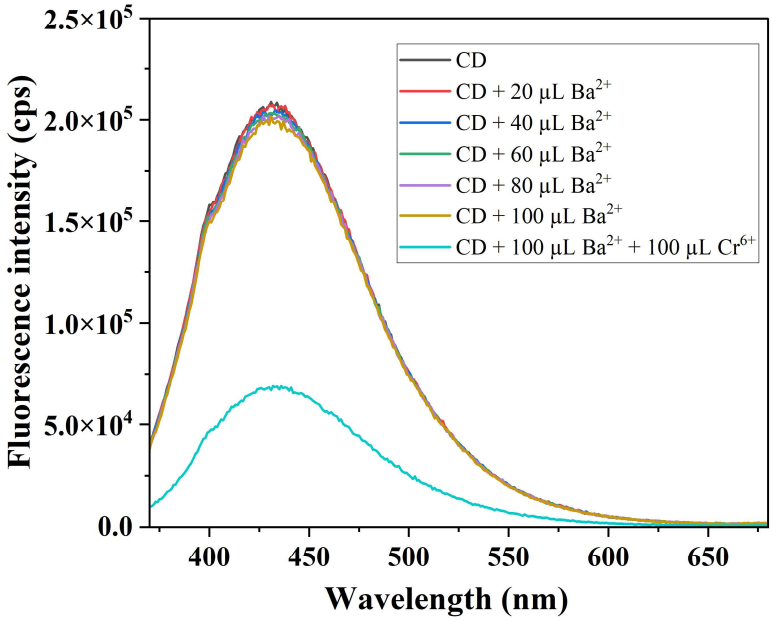

Figure S16. Fluorescence response of CDs upon addition of 100 µL 2mM Ba^{2+} solution and 100 µL 2 mM Cr^{6+} solution (λ_{ex}= 350 nm).

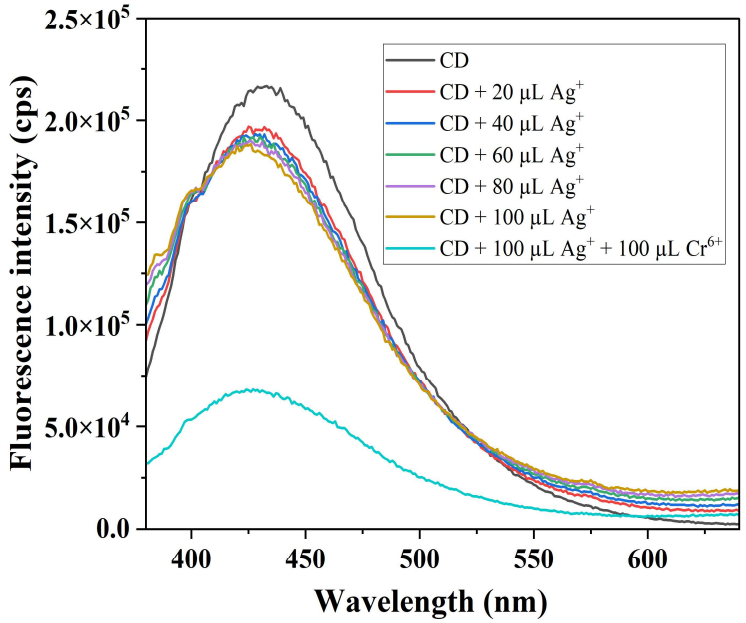

Figure S17. Fluorescence response of CDs upon addition of 100 µL 2mM Ag^{+} solution and 100 µL 2 mM Cr^{6+} solution (λ_{ex}= 350 nm).

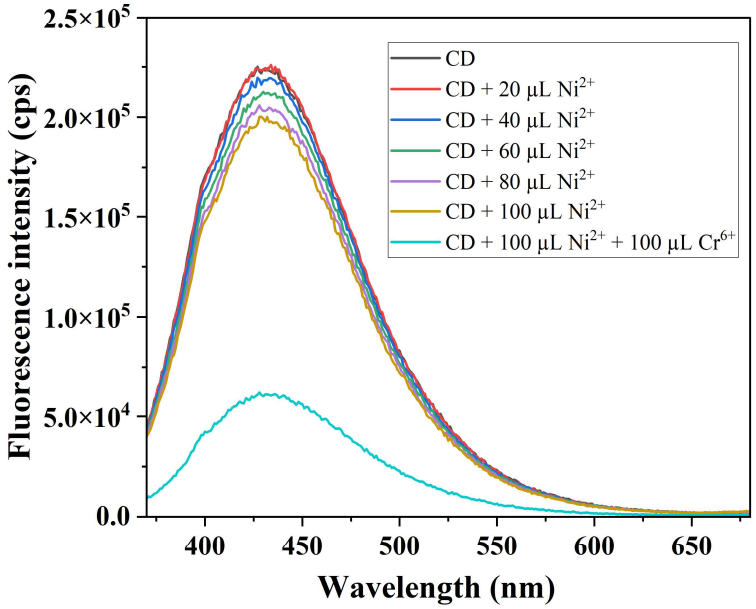

Figure S18. Fluorescence response of CDs upon addition of 100 µL 2mM Ni^{2+} solution and 100 µL 2 mM Cr^{6+} solution (λ_{ex}= 350 nm).

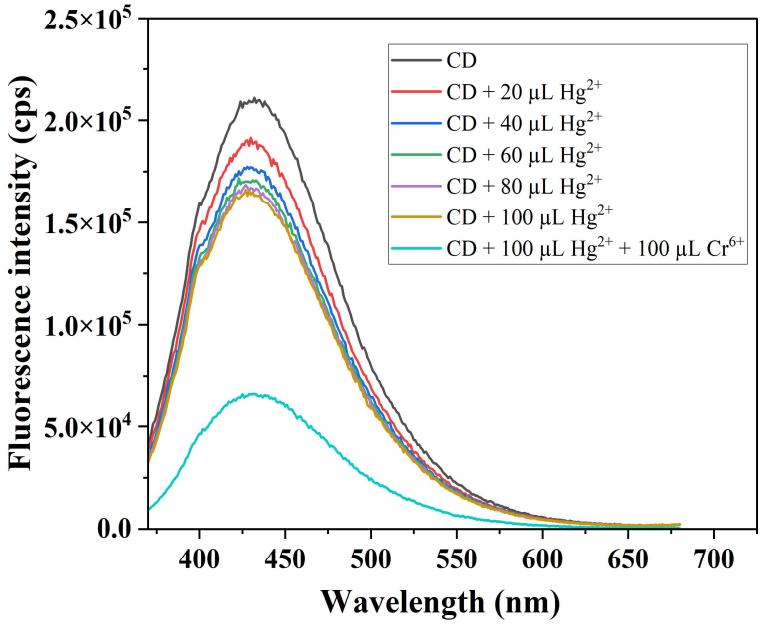

Figure S19. Fluorescence response of CDs upon addition of 100 µL 2mM Hg^{2+} solution and 100 µL 2 mM Cr^{6+} solution (λ_{ex}= 350 nm).

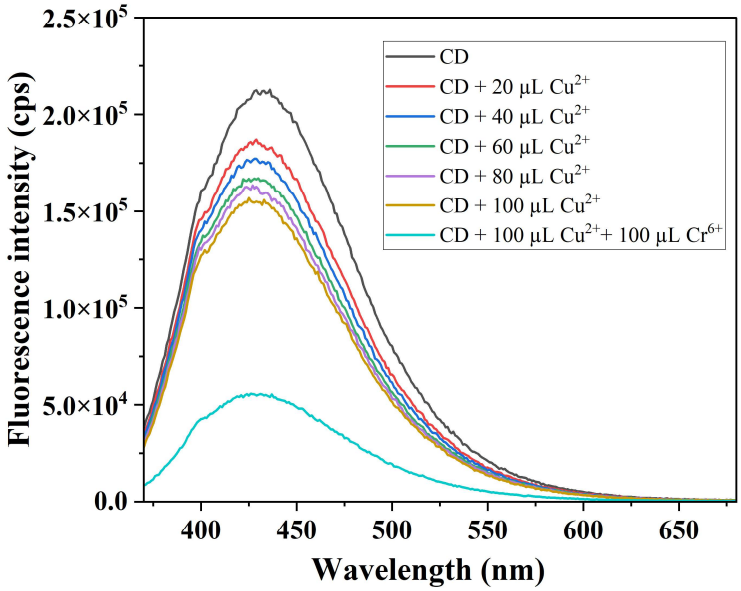

Figure S20. Fluorescence response of CDs upon addition of 100 µL 2mM Cu^{2+} solution and 100 µL 2 mM Cr^{6+} solution (λ_{ex}= 350 nm).

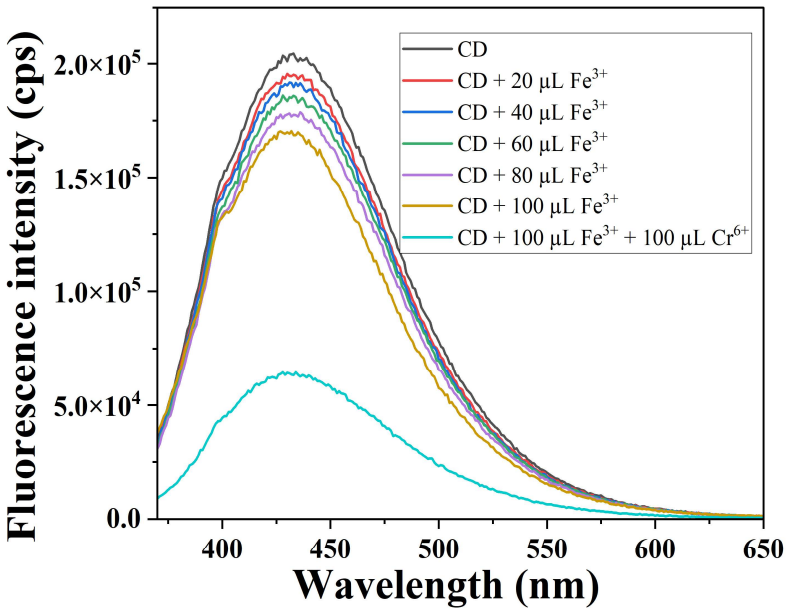

Figure S21. Fluorescence response of CDs upon addition of 100 µL 2mM Fe^{3+} solution and 100 µL 2 mM Cr^{6+} solution (λ_{ex}= 350 nm).

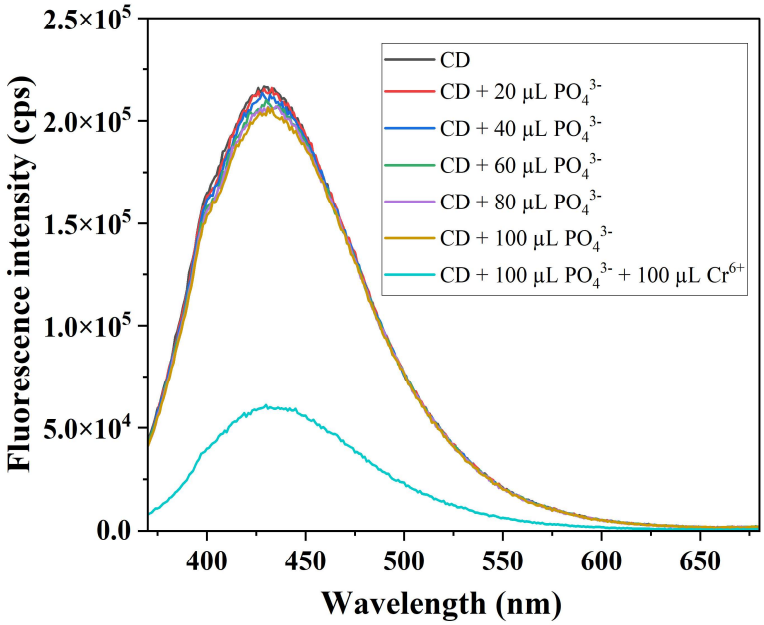

Figure S22. Fluorescence response of CDs upon addition of 100 µL 2mM PO_4^{3-} solution and 100 µL 2 mM Cr^{6+} solution (λ_{ex}= 350 nm).

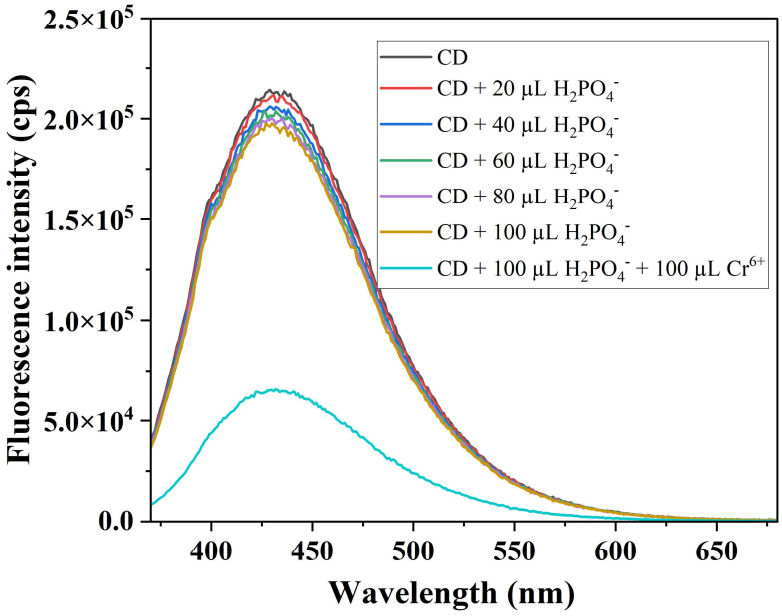

Figure S23. Fluorescence response of CDs upon addition of 100 µL 2mM $H_2PO_4^-$ solution and 100 µL 2 mM Cr^{6+} solution (λ_{ex}= 350 nm).

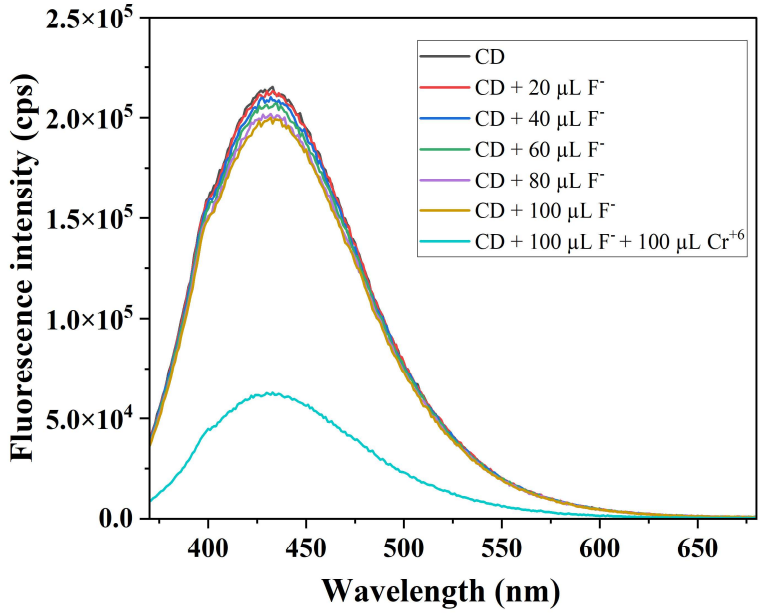

Figure S24. Fluorescence response of CDs upon addition of 100 µL 2mM F^- solution and 100 µL 2 mM Cr^{6+} solution (λ_{ex}= 350 nm).

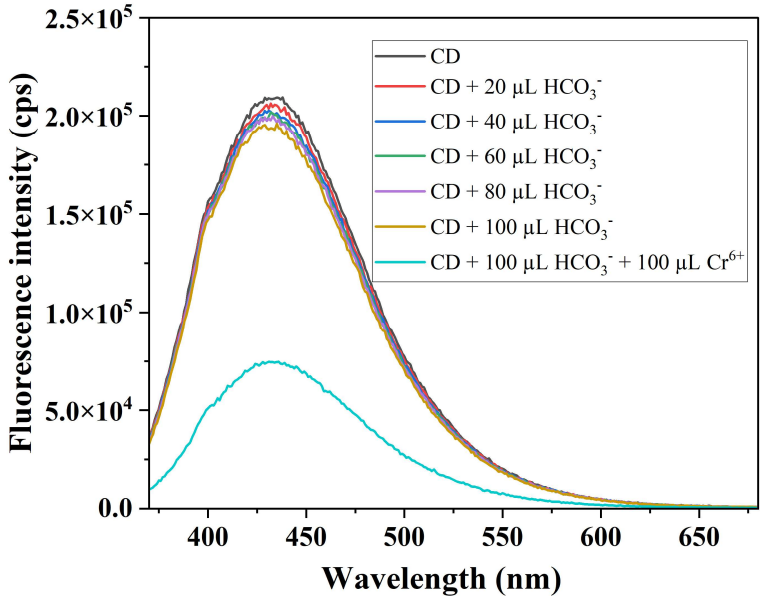

Figure S25. Fluorescence response of CDs upon addition of 100 µL 2mM HCO_3^- solution and 100 µL 2 mM Cr^{6+} solution (λ_{ex}= 350 nm).

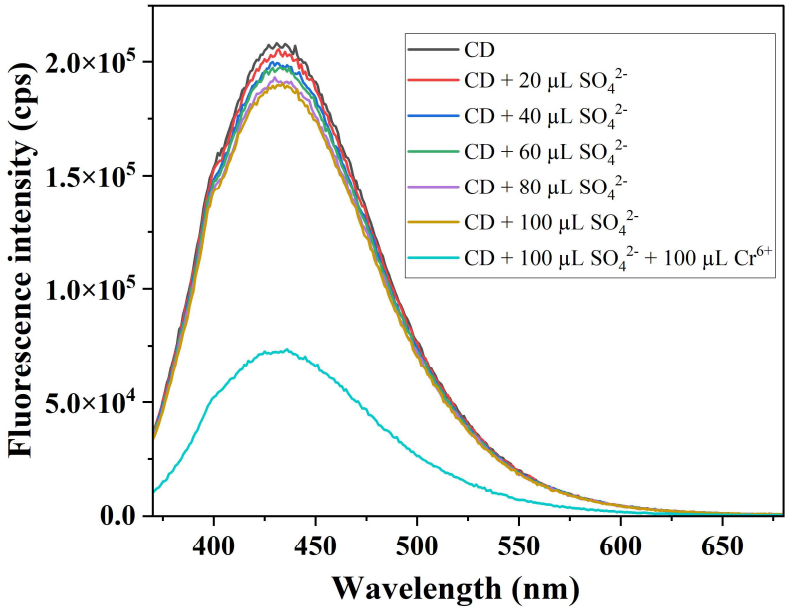

Figure S26. Fluorescence response of CDs upon addition of 100 µL 2mM SO_4^{2-} solution and 100 µL 2 mM Cr^{6+} solution (λ_{ex}= 350 nm).

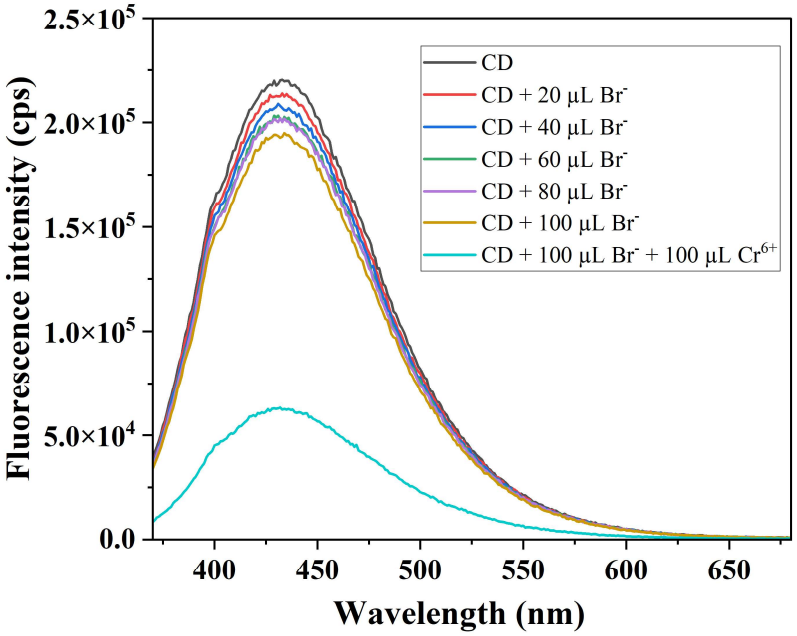

Figure S27. Fluorescence response of CDs upon addition of 100 µL 2mM Br^- solution and 100 µL 2 mM Cr^{6+} solution (λ_{ex}= 350 nm).

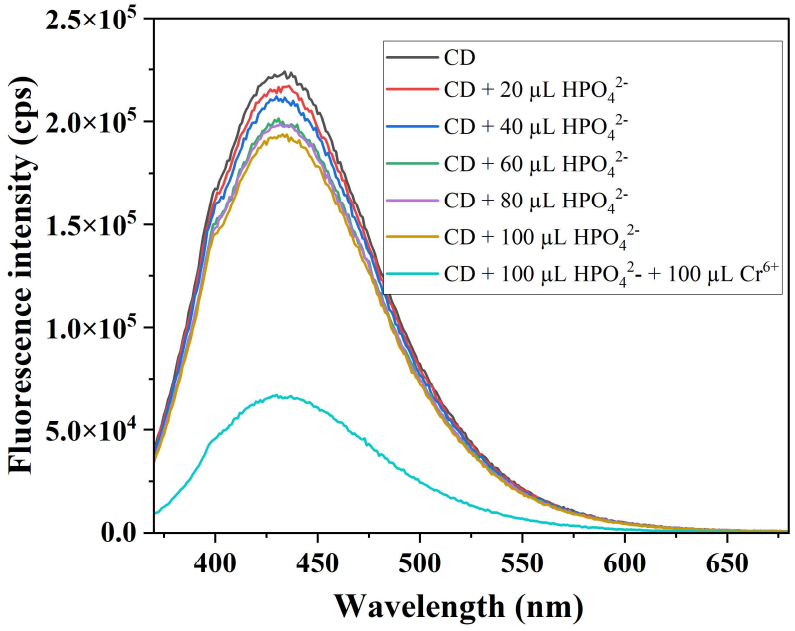

Figure S28. Fluorescence response of CDs upon addition of 100 µL 2mM HPO_4^{2-} solution and 100 µL 2 mM Cr^{6+} solution (λ_{ex}= 350 nm).

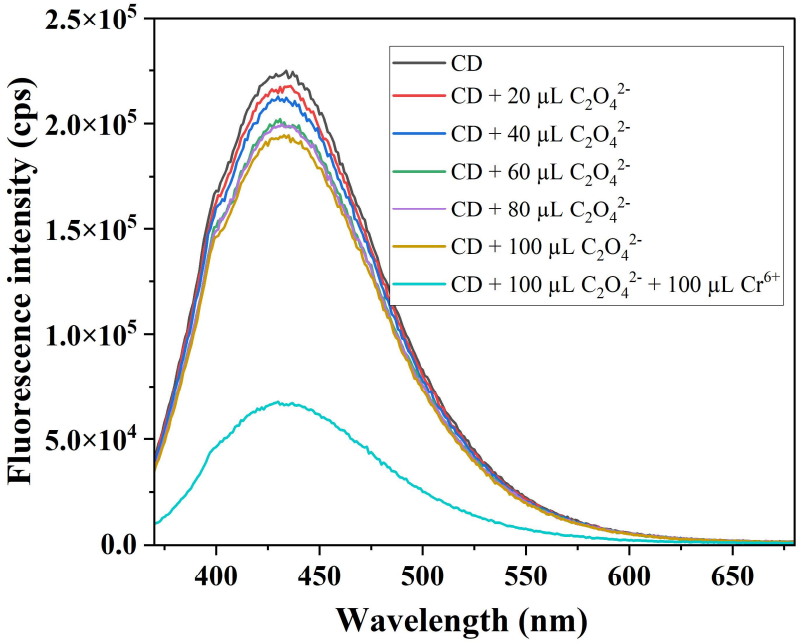

Figure S29. Fluorescence response of CDs upon addition of 100 µL 2mM $C_2O_4^{2-}$ solution and 100 µL 2 mM Cr^{6+} solution (λ_{ex}= 350 nm).

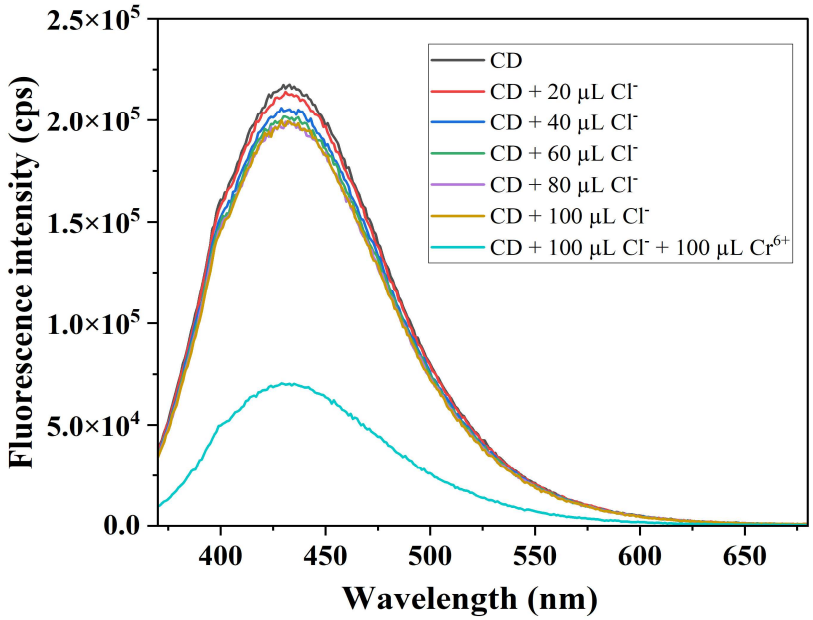

Figure S30. Fluorescence response of CDs upon addition of 100 µL 2mM Cl^- solution and 100 µL 2 mM Cr^{6+} solution (λ_{ex}= 350 nm).

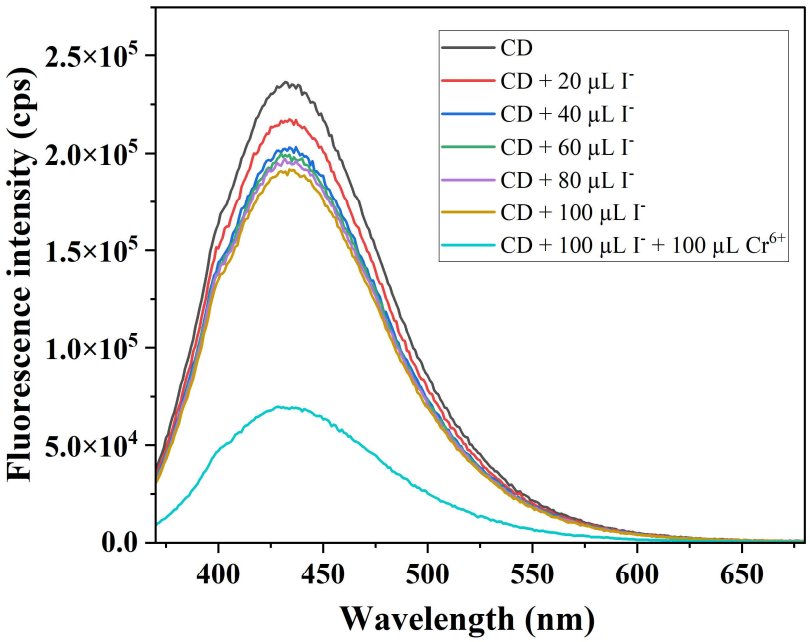

Figure S31. Fluorescence response of CDs upon addition of 100 μL 2mM I^- solution and 100 μL 2 mM Cr^{6+} solution (λ_{ex}= 350 nm).

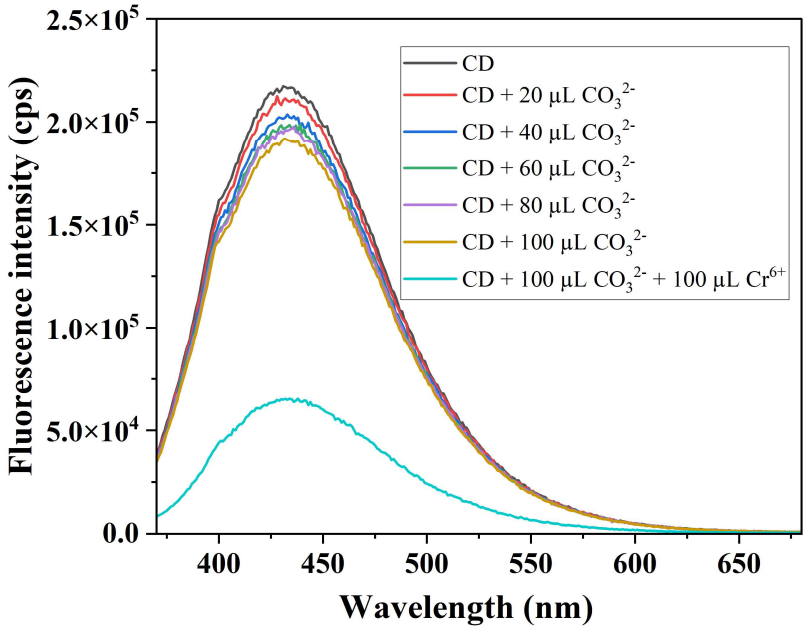

Figure S32. Fluorescence response of CDs upon addition of 100 μL 2mM CO_3^{2-} solution and 100 μL 2 mM Cr^{6+} solution (λ_{ex}= 350 nm).

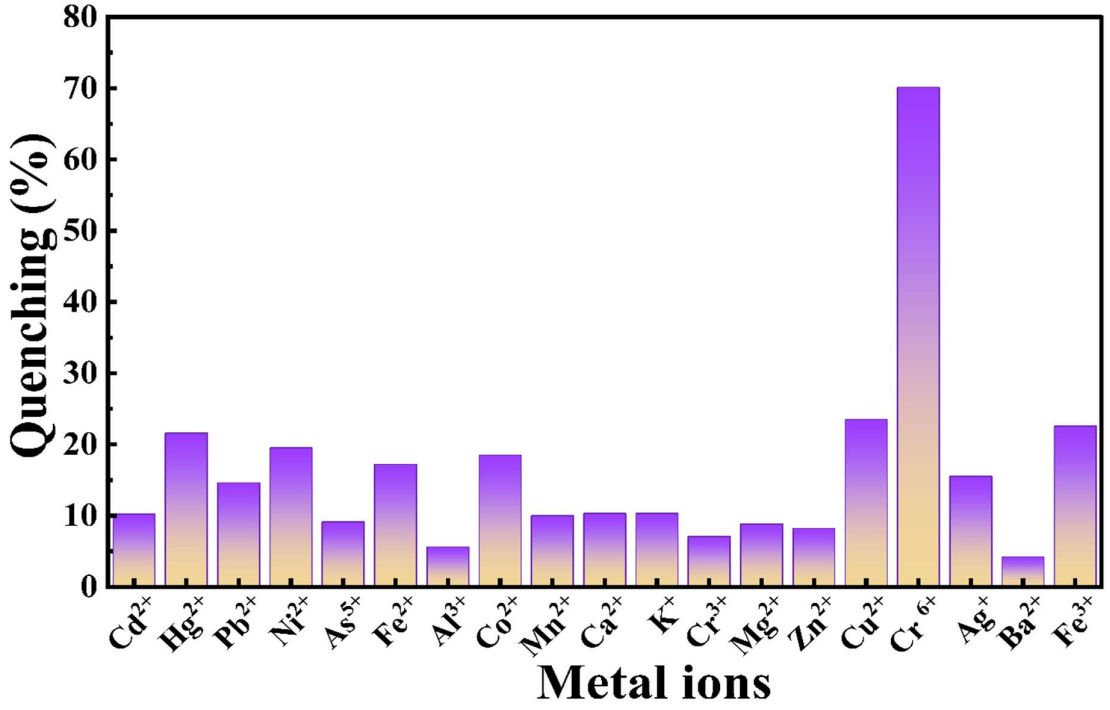

Figure S33. Percentage of fluorescence quenching in CDs upon addition of various metal ions.

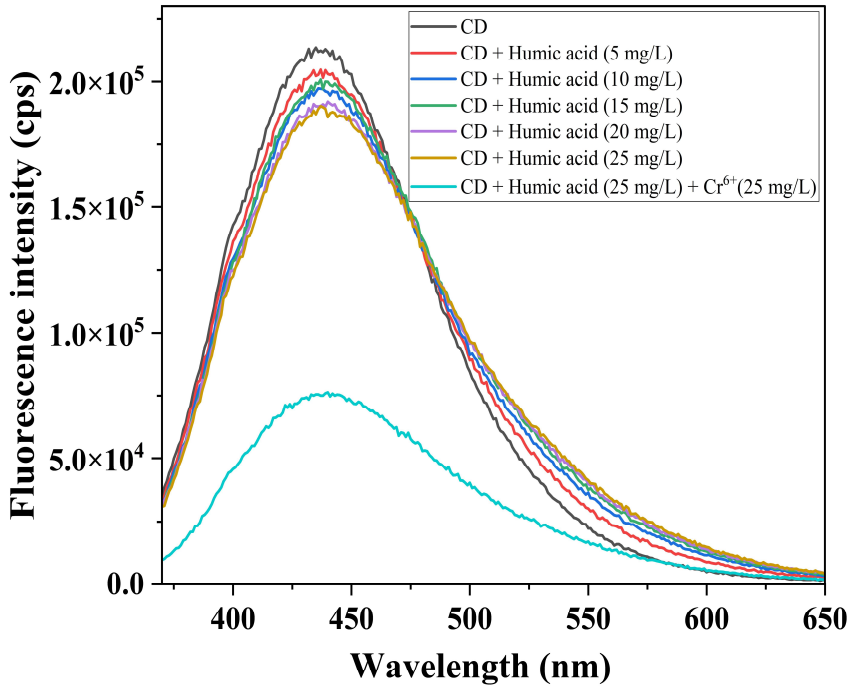

Figure S34. Fluorescence response of CDs upon addition of humic acid (25 mg/L) solution and Cr^{6+} (25 mg/L) solution (λ_{ex}= 350 nm).

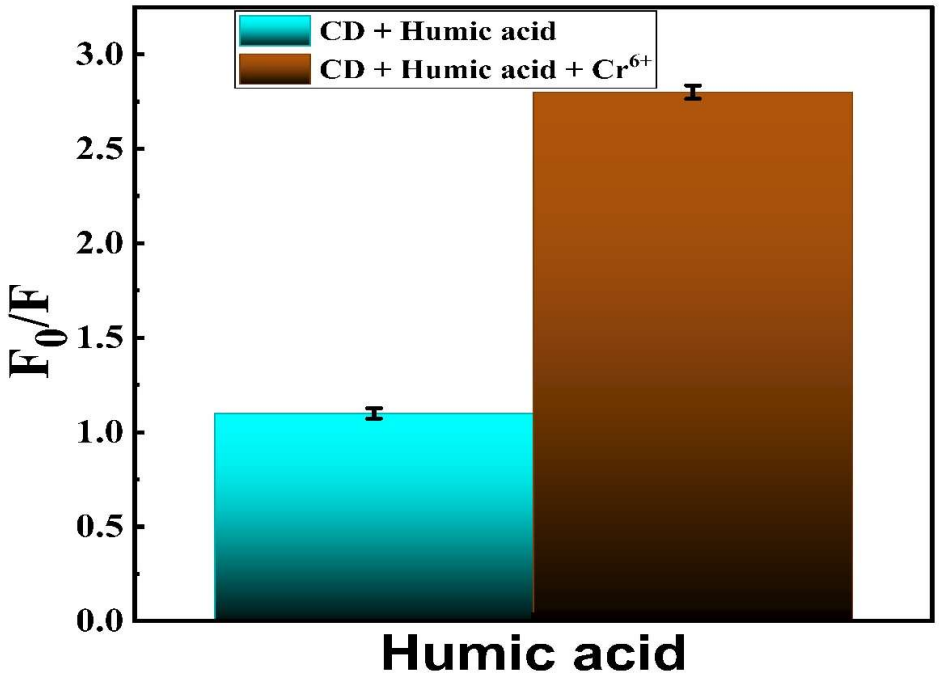

Figure S35. Interference study of humic acid in the sensing of Cr^{6+} by NB24@CDs.

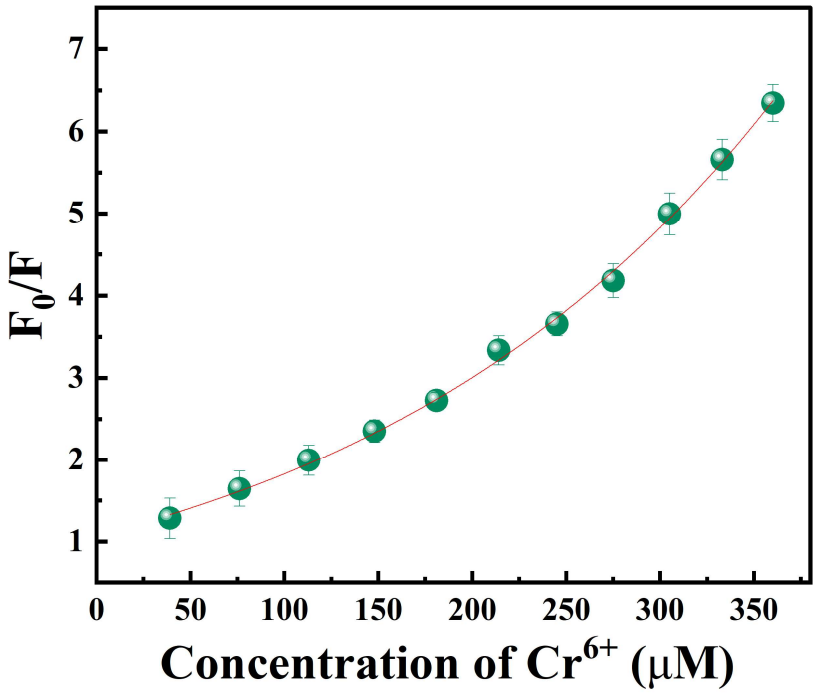

Figure S36. Stern-Volmer plot for fluorescence quenching of CDs against Cr^{6+} concentration in micromolar.

Temperature	K_{SV} ($\times 10^5$ M^{-1})	RSD (%)
25°C	6.20 ± 0.18	2.6
35°C	5.40 ± 0.16	3.1
55°C	4.20 ± 0.17	3.9

Table S1. K_{SV} obtained from Stern-Volmer plots at different temperatures, indicating decreasing values with increasing temperatures (n = 3).

Water type	Spiked (nM)	Recovered (nM)	Recovery %	RSD %
Tap	39	37.908	97.2	1.98
	77	74.767	97.1	2.17
	113	111.305	98.5	1.56
	148	146.372	98.9	1.92
	181	183.353	101.3	3.12
River	39	38.6217	99.03	2.55
	77	75.922	98.6	2.69
	113	111.644	98.8	1.37
	148	147.112	99.4	3.02

	181	180.276	99.6	2.12
Lake	39	38.103	97.7	1.06
	77	75.383	97.9	1.82
	113	110.514	97.8	2.07
	148	146.076	98.7	1.84
	181	179.19	99	2.94

Table S2. Determination of Cr^{6+} in real samples using CDs as fluorescent probe (n = 3).

Precursors	Method	LOD	Reference
Lignocellulosic biomass (banana stem) and phosphoric acid	Hydrothermal	2.4 μM	[1]
Syzygium cumini juice and betaine	Hydrothermal	0.033 μM	[2]
Cellulose acetate and p-phenylenediamine	Hydrothermal	0.0303 μM	[3]
Zinc acetate and cinnamon	Hydrothermal	3.97 μg/mL	[4]
Mature green leaves	Hydrothermal	0.004 mg/L	[5]
Lycium barbarum	Hydrothermal	0.16 μM	[6]
Lignin, o-phenylenediamine, Nickel (II) chloride hexahydrate, EDTA-2Na	Hydrothermal	0.17 μM	[7]
$(NH_4)_2HPO_4$ and m-phenylenediamine, and terephthalic acid	Solvothermal	0.59 μM	[8]
Tartaric acid and tryptophan	Hydrothermal	0.51 μM	[9]
M-phenylenediamine and copper acetylacetonate	Solvothermal	0.34 μM	[10]
O-phenylenediamine and copper acetylacetonate	Solvothermal	0.4 μM	[10]
This work	Hydrothermal	30 nM	

Table S3. Comparison of some recently published platforms for the detection of Cr^{6+}.

References

1. Goswami J, Rohman SS, Guha AK, Basyach P, Sonowal K, Borah SP, Saikia L, Hazarika P. Phosphoric acid assisted synthesis of fluorescent carbon dots from waste biomass for detection of Cr (VI) in aqueous media. *Materials chemistry and Physics*., 2022, **286**, 126133.

2. Behera L, Naik AK, Sahu BB, Mohapatra S. Betaine-Modified Green Carbon Dot for Cr (VI) Sensing, in Vivo Cr (VI) Imaging, and Growth Promotion in the Rice Plant. *ACS Applied Bio Materials*., 2024, **7**, 7624.
3. Li YF, Zhang X, Lu Q, Cao JZ, Gao S, Liu QZ, Cai XX, Zhao H. Cellulose-based yellow-green emitting carbon dots with large Stokes shift as effective "turn off-on" fluorescence platforms for Cr (VI) and AA dual efficacy detection. *Analytica Chimica Acta*., 2024, **1324**, 343102.
4. Kolekar AG, Nille OS, Koparde SV, Patil AS, Waghmare RD, Sohn D, Anbhule PV, Kolekar GB, Gokavi GS, More VR. Green, facial zinc doped hydrothermal synthesis of cinnamon derived fluorescent carbon dots (Zn-Cn-CDs) for highly selective and sensitive Cr6+ and Mn7+ metal ion sensing application. *Spectrochimica Acta Part A: Molecular and Biomolecular Spectroscopy*., 2024, **304**, 123413.
5. Patra S, Golder AK, Uppaluri RV. Green synthesis of carbon dots from mature green tea leaves for label-free fluorescence sensing of chromium (VI). *Optical Materials*., 2024, **154**, 115767.
6. Xie J, Wu Z, Sun J, Lv C, Sun Q. Green synthesis of carbon quantum dots derived from Lycium barbarum for effective fluorescence detection of Cr (VI) sensing. *Journal of Fluorescence*., 2024, **34**, 571.
7. Chen Y, Wang Z, Liang M, Liu Y, Dong W, Hu Q, Dong C, Gong X. High-efficient nickel-doped lignin carbon dots as a fluorescent and smartphone-assisted sensing platform for sequential detection of Cr (VI) and ascorbic acid. *International Journal of Biological Macromolecules*., 2024, **274**, 133790.
8. Tian Y, Yue Y. Phosphor doped carbon dots with high photoluminescence and stability towards pH and Cr (VI) sensors. *Microchemical Journal*., 2024, **207**, 112046.
9. Chen H, Li D, Zheng Y, Wang K, Zhang X, Zhou S, Wei S, Yong F, Nie J, Wen H, Wu J. Metal-free carbon-dots nanozyme with oxidase-like activity as photocatalysts for highly efficient detection/reduction of Cr (VI) and antibacterial application. *Separation and Purification Technology*., 2025, **356**, 129852.
10. Hao X, Zhang X, Liu C, Yang P. Nanoarchitectonics of Cu-derived bright carbon dots towards Cr (VI) and tetracycline hydrochloride detection. *Applied Surface Science*., 2025, **687**, 162217.